ANNALI DI GEOFISICA, VOL. XXXVII, N. 5, September 1994

Large teleseismic *P*-wave residuals observed at the Alban Hills volcano, Central Italy

Giovanni Battista Cimini([1]), **Claudio Chiarabba**([1]), **Alessandro Amato**([1]) **and H. Mahadeva Iyer**([2])
([1]) *Istituto Nazionale di Geofisica, Roma, Italy*
([2]) *U.S. Geological Survey, Menlo Park, CA, U.S.A.*

Abstract
We collected teleseismic waveforms from a digital microseismic network deployed by the Istituto Nazionale di Geofisica (ING) in collaboration with the U.S. Geological Survey (USGS), on the Alban Hills Quaternary volcano during the 1989-1990 seismic swarm. About 50 events were recorded by the network, 30 of them by at least 4 stations. We analysed the data in order to image crustal heterogeneities beneath the volcano. The results show large delay time residuals up to ~ 1 second for stations located on the volcano with respect to station CP9 of the National Seismic Network located about 20 km to the east on the Apennines. This suggests that the whole area overlies a broad low-velocity region. Although the ray coverage is not very dense, we model the gross seismic structure beneath the volcano by inverting the teleseismic relative residuals with the ACH technique. The main features detected by the inversion are a low-velocity zone beneath the southwestern flank of the volcano, and a high-velocity region beneath the center. The depth extension of these anomalous zones ranges between 5 and 16 km. The correspondence between the low-velocity region and the most recent activity of the volcano (~ 0.027 Ma) leads us to infer the presence of a still hot magmatic body in the crust beneath the southwestern side of the volcano, whereas the central part overlies the older and colder high-velocity volcanic roots related to the previous central activity (0.7 to 0.3 Ma).

Key words *travel time residual – teleseismic tomography – Alban Hills*

1. Introduction

The Alban Hills volcano (*Vulcano Laziale*) is a Quaternary volcano located along the Tyrrhenian margin of the Central Apennines, about 20 km southeast of Rome (fig. 1). It consists of high-*K* volcanic sites, which were emplaced from about 0.7 Ma to 0.027 Ma (Fornaseri, 1985) during three main eruptive phases. The first phase consisted of the eruption of more than 270 km^3 of mostly pyroclastic flows from a central cone during four separate eruptions, along with the formation of a large caldera by repeated magma chamber collapse (~ 0.4 Ma) (Bertagnini *et al.*, 1985; De Rita *et al.*, 1988). The second phase started inside the caldera with the build-up of a second central cone (~ 0.30 Ma) (De Rita *et al.*, 1988). Phreato-magmatic explosions from several eccentric cones, mostly located in the western side of the volcano, characterize the most recent activity (~ 0.027 Ma, see fig. 1) (De Rita *et al.*, 1988).

Information on the deep structure of the volcano is very poor. The few data available include shallow (1-2 km) refraction lines (Amato and Valensise, 1986) and gravity data (Toro, 1977), both indicating the presence of carbonate rocks, analogous to those outcropping in the nearby Apennines, in the upper crust. Seismicity in the Alban Hills is available since the Roman Age. Several seismic swarms

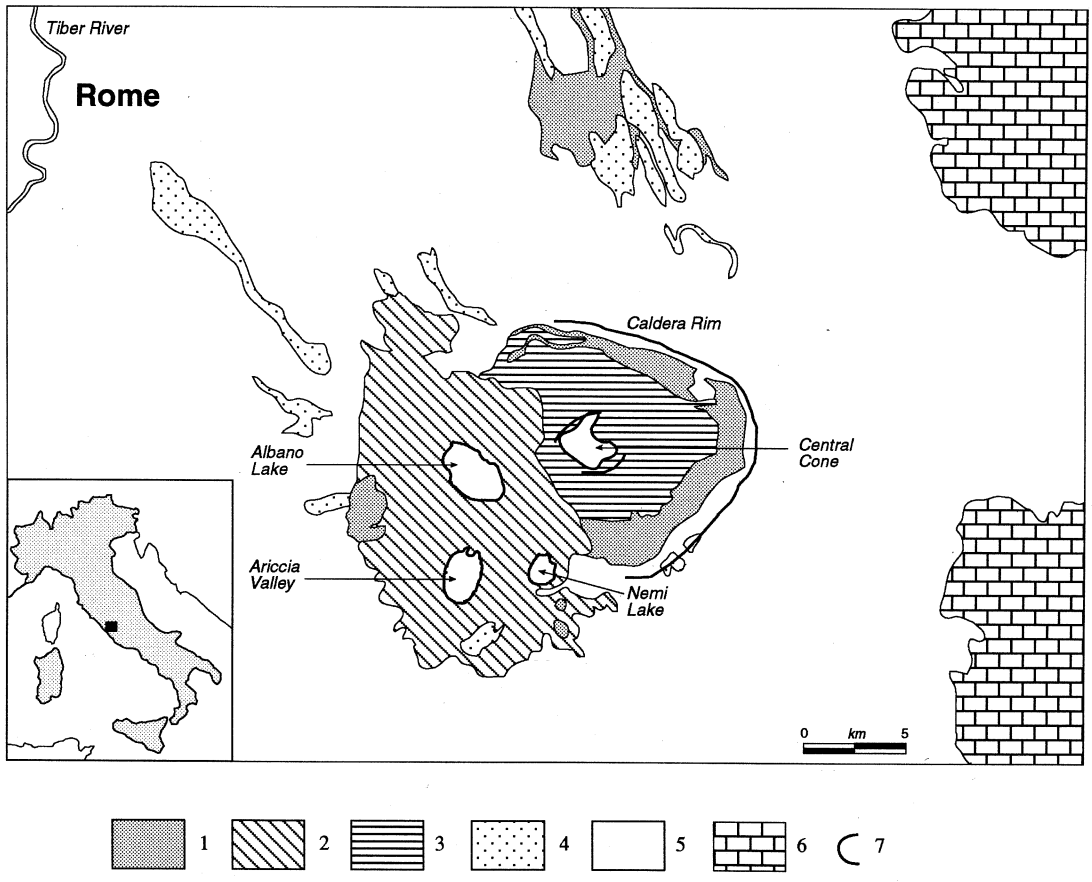

Fig. 1. Geologic map of the Alban Hills volcano. 1) Continental terrains; 2) phreato-magmatic products of the third (most recent) phase (0.2-0.03 Ma); 3) pyroclastic products of the second phase (0.3 - 0.2 Ma); 4) lava flows of the first phase (0.7 - 0.3 Ma); 5) pyroclastic rocks of the first phase (0.7 - 0.3 Ma); 6) Meso-Cainozoic limestone formations of the Apenninic chain; 7) Caldera rim, central cone and explosive craters.

occurred in the last 300 years with duration ranging between a few days and two years (Molin, 1981). On April 13 1989, a M_D 3.2 earthquake marked the onset of a 1 year long shallow seismic swarm. Earthquake hypocenters computed for more than 1100 events of this swarm are concentrated in the western side of the volcano, to a depth of 6 km (Amato *et al.*, 1994). Three-dimensional *P*- and *S*-wave velocity structure computed by inversion of local earthquake arrival times reveals high velocity anomalies in the upper 6 km beneath the volcano (Chiarabba *et al.*, 1994). These anomalies have been interpreted as uplifted carbonate units, possibly thermally metamorphosed at depth due to the proximity of a cooling shallow magma chamber in the western and youngest side of the volcano.

In order to image the crustal structure beneath the volcano, and to extend to greater depth the information inferred from local earthquake tomography for the uppermost crust (Chiarabba *et al.*, 1994), we studied the distribution of relative teleseismic traveltime residu-

als and calculated a 3-D tomographic inversion following the ACH scheme (Aki *et al.*, 1977). The teleseismic events were recorded by a digital seismic network, deployed in the Alban Hills area by ING in collaboration with the USGS during the 1989-1990 seismic swarm. Digital seismograms from the permanent stations RMP, RDP, and CP9, of the National Centralized Seismic Network (RSNC) were also used in the analysis. The digital network shown in fig. 2, consisted of stations equipped with either short period (Teledyne S-13 and Mark L4-C) or broadband (Guralp CMG3) seismometers.

2. Data Analysis

Out of 46 teleseisms detected by the seismic network operating in the study area during one year, we selected 24 *P* events (distance range 25°-100°) and 6 *PKP* events (distance range 110°-180°), which provided a total of 160 arrival times. The NEIC locations of these events, with magnitudes m_b ranging between 5.1 and 6.4, are shown in fig. 3. Although the number of events is small, their geographic distribution is relatively homogeneous, with teleseismic wavefronts approaching the network from a wide range of azimuths. The availability of high-quality digital seismograms allowed us to achieve a high precision in the picking of teleseismic phases and in the computation of travel time residuals.

We analised the teleseismic waveforms by means of an interactive graphic procedure (Amato *et al.*, 1993). This procedure allows us to visualize groups of waveforms recorded at different stations, and to align the seismograms

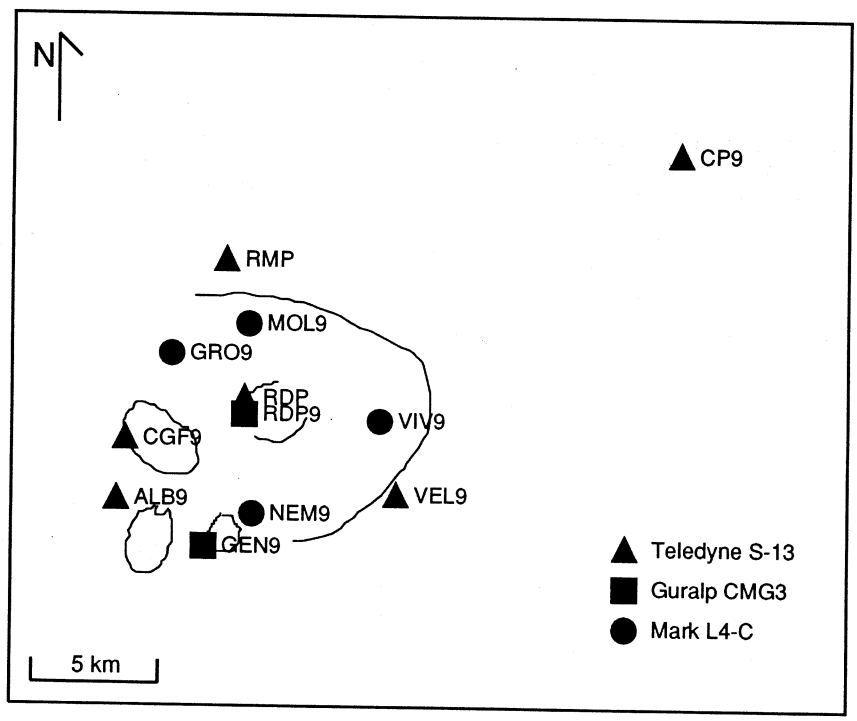

Fig. 2. Station distribution of the National Seismic Network (RMP, RDP, and CP9), and of the digital temporary network operating in the Alban Hills area during the 1989-1990 seismic swarm. Stations CP9, RMP, GRO9, VIV9, MOL9 had a single component vertical sensor, all the other had three-component sensors.

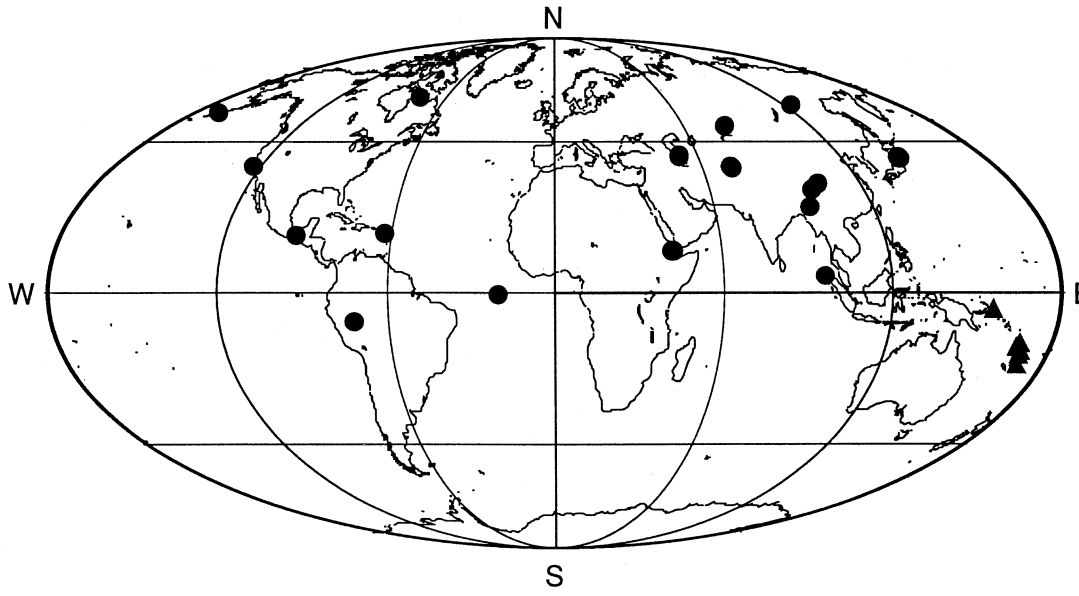

Fig. 3. NEIC location of the *P* (solid circles) and *PKP* (solid triangles) events used in this study.

of each event using digital band-pass filtering, amplitude and time scaling, and visual correlation. This analysis of the digital seismograms allows the correct identification of the arrival time of the teleseismic phases, avoiding problems due to early arrivals of diffracted phases, the presence of reverse polarities or emergent arrivals, and cycle skipping (Cimini and Amato, 1993; Evans and Achauer, 1993). As an example, fig. 4 shows the aligned waveforms for a deep earthquake occurred in Brazil (May 5, 1989; $m_b = 6.4$; $z = 593$ km). Broadband signals have been band-pass filtered to correlate them with waveforms recorded by short period instruments. The consistency of this procedure has been checked comparing waveforms at one site (station RDP) where both instruments were installed.

For each seismic ray, we determine the arrival time T_{ij}, where i is the event and j the station. A correction (Δt) for site elevation h, is applied to each observed arrival time according to the formula $\Delta t = \Delta h \cos i_0 / v_p$, where i_0 is the incidence angle at the station, and $v_p = 2.5$ km/s. Timing errors on T_{ij} are estimated to be approximately ± 0.02 s.

We compute the absolute residuals R_{ij}, *i.e.* the difference between the observed travel time and the theoretical travel time H_{ij}, determined using the Herrin tables (Herrin, 1968), according to

$$R_{ij} = T_{ij} - T_{oi} - H_{ij} \qquad (2.1)$$

where T_{oi} is the origin time of the $i-th$ event.

To reduce the effects of hypocentral mislocation, origin time error, approximation to a standard Earth model, and the shift between first arrival and selected picking time, we compute the residuals relative to the mean of the network for each particular event as

$$R_{ij}^{rel} = R_{ij} - \frac{1}{\sum_{j=1}^{Ni} W_{ij}} \sum_{j=1}^{N_i} W_{ij} R_{ij} \qquad (2.2)$$

where N_i is the number of observations of the $i-th$ event, the second term to the right end of eq. (2.2) is the weighted mean residual of the

net (R_i) and W_{ij} is a subjective estimate of the single onset time quality (see Ellsworth and Koyanagi, 1977; Evans and Zucca, 1988).

In order to estimate velocity heterogeneities on a broader scale, we also compute the residuals relative to station CP9 of the National Seismic Network of ING, located 20 km off the volcano, by

$$R_{ij}^{rel} = R_{ij} - R_{i\,\mathrm{CP9}} \qquad (2.3)$$

where $R_{i\,\mathrm{CP9}}$ is the absolute residual at this reference station. The location of station CP9, on Mesozoic limestones about 20 km to the east of the volcano, ensures us that ray paths reaching CP9 do not travel in the crust beneath the volcano. By doing so, we avoid errors due to instability of the mean (R_i), as each event may be recorded by a slightly different combination of stations.

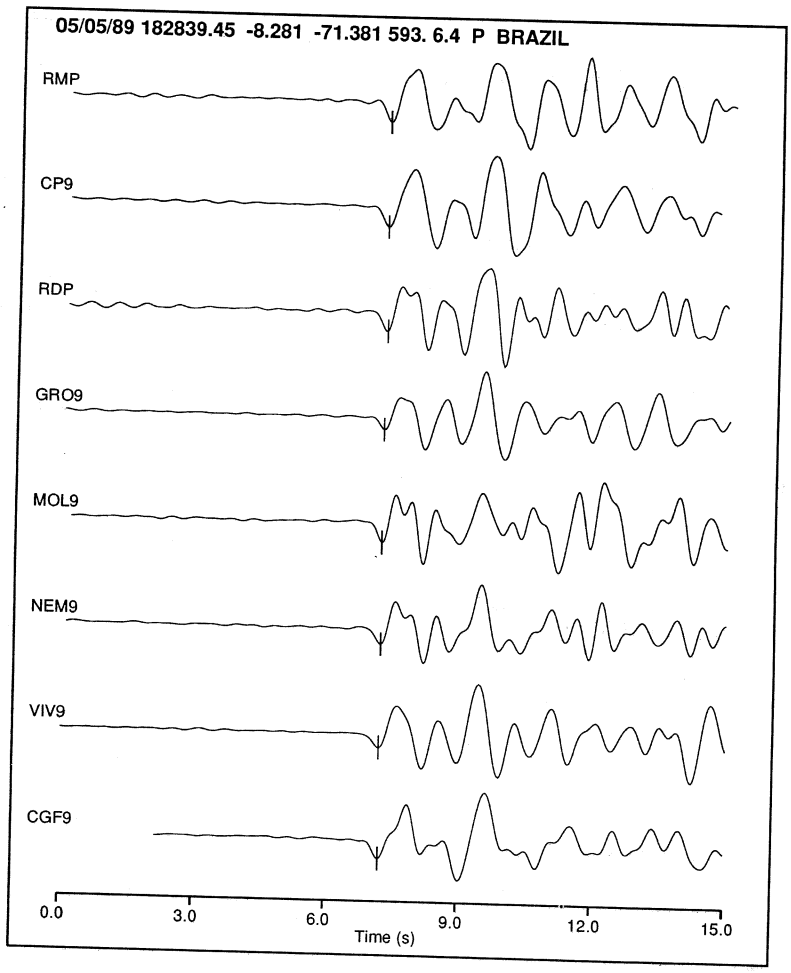

Fig. 4. Alignment of the digital waveforms of a *P* teleseism (May 5, 1989; Brazil, $m_b = 6.4$) as obtained by means of the interactive graphic procedure.

3. Distribution of the teleseismic residuals

The relative residual distribution versus azimuth and angle of incidence (or distance) of teleseismic rays, can be used to qualitatively delineate anomalous regions at depth (Steeples and Iyer, 1976). Shallow velocity anomalies beneath the array produce a residual pattern that is largely independent of the direction and vertical incidence of the approaching rays, since all rays travel through the anomalous structure to reach the station.

On the contrary, a deeper heterogeneous body produces residuals that are more sensitive to the azimuth and angle of incidence of the incoming wavefronts, since not all rays pass through it. For instance, a high-velocity anomaly at depth displays travel time residuals that are lower than ones computed for rays travelling through the surrounding homogeneous medium (Harris *et al.*, 1991; Amato *et al.*, 1993).

As a first indication of the variation in the teleseismic propagation beneath the Alban Hills volcano, fig. 5a,b shows the relative residual distribution of the *P* and *PKP* phases computed for all the azimuthal directions (0°-360°). The pattern, similar for the two different data sets, reveals the presence of an area southwest of the volcano where strong delays occur (positive values), and a zone in the north-eastern part with early arrivals (negative values). Between these two regions, we observe a difference in the mean residuals as large as 0.41 s.

A more detailed view of the azimuthal variation of the *P* travel time residual in the area can be obtained by looking at groups of events divided in sectors of 90° (figs. 6 and 7). The mean relative residuals (computed by formulas 2 and 3 respectively) for teleseismic rays approaching from the NE (upper right), SE, SW and NW (upper left), are plotted. For reference, we plot in the central panel the mean values for all the *P* events (fig. 5a).

The main feature is the systematic pattern of positive residuals in the southwestern part of the Alban Hills region, below the Albano and Nemi craters (fig. 1). Here, positive residuals as large as 0.30 s (fig. 6), or 1.00 s with respect to reference station CP9 (fig. 7), are observed for events approaching from the SE quadrant. The separation between an area of late arrivals (*i.e.*, low velocity) beneath the western side of the volcano, and an area of early arrivals (*i.e.*, high velocity) is more evident for events approaching from NW or SE and less clear from NE and SW. This may reflect a heterogeneous structure in the lower crust or upper mantle beneath the Alban Hills volcano, with a NW-SE orientation. Furthermore, fig. 7 indicates that delays are observed for all the stations on the volcano relatively to the Apenninic station CP9.

This behaviour is opposite to that expected from the Moho trend, which deepens moving from the Thyrrenian Sea toward the Apenninic chain. Unfortunately the network width, designed mainly for locating local earthquakes, is too small to allow us to constrain the extension of anomalies at depth.

Finally, fig. 8a-c shows the residual variation (determined by eq. (2.2) for three stations located in the study area approximately along a North-South direction (see fig. 2).

In fig. 8a the residual distribution of station RMP shows no significant azimuth-distance dependence and a slight negative offset. This pattern is consistent with a weak shallow high-velocity anomaly. The residual plot for station RDP (fig. 8b) is an example of a very insensitive spatial variation, except for the presence of one scattered negative value (– 0.39 s). This value is relative to a Vanuatu Islands earthquake, which we have analised as PKP_{AB} phases according to the Herrin reference model (Herrin, 1968). For this earthquake we note increasing residuals at increasing epicentral distances; so we conclude that the PKP_{AB} branch is not an appropriate fit to the arrival times of the recorded seismograms, and is most probably the PKP_{BC} branch (Amato *et al.*, 1993). We have not used this event in the subsequent inversion. The third plot (fig. 8c) shows the residual distribution for station GEN9, located in the southwestern border of the Alban Hills region. Here we observe a substantially systematic pattern of late arrivals, indicating low velocity at shallow depth.

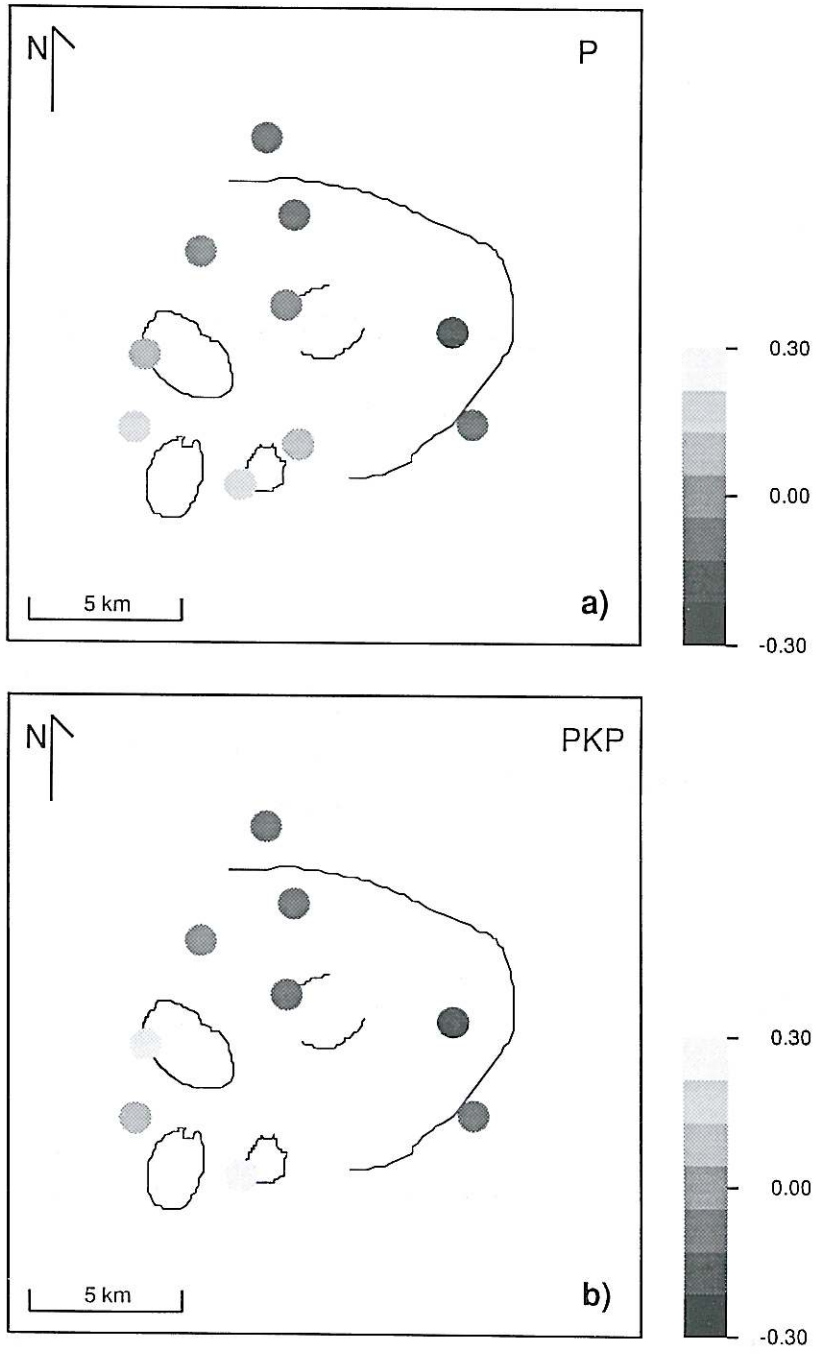

Fig. 5a,b. Mean relative residuals over the network determined for (a) *P* and (b) *PKP* phases for the whole azimuthal range (0°-360°). Note the strong similarity between the two different data sets.

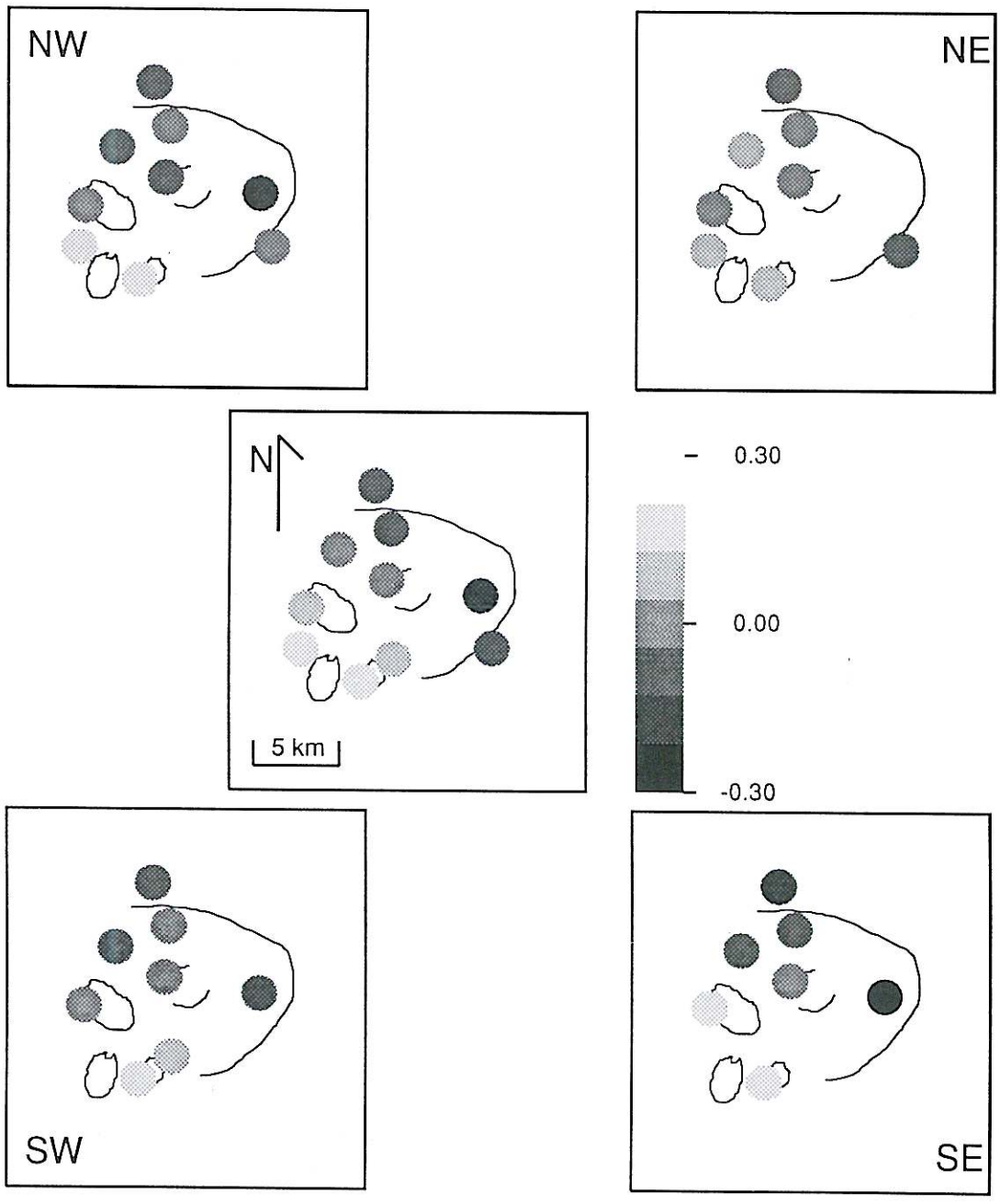

Fig. 6. Mean relative residuals computed for the *P* events grouped in NW, NE, SE, SW approaching directions. In the central map the distribution of the azimuthally independent residuals (invariant) of fig. 5a is shown. A region of strong delays (up to 0.3 s.) is present in the southwestern part of the volcano, whereas the center and the eastern side are characterized by early arrival times.

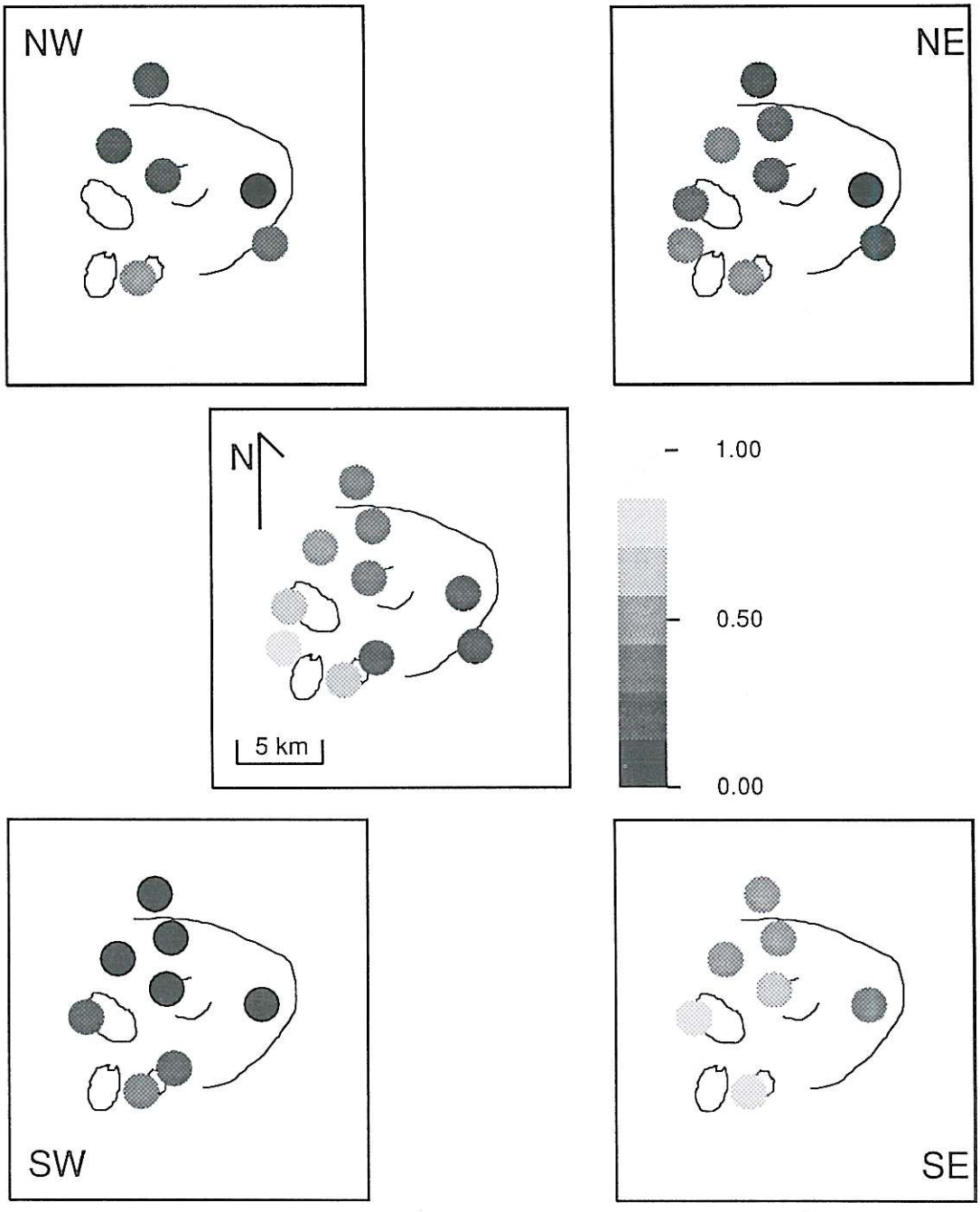

Fig. 7. Same as fig. 6, with residuals computed with respect to CP9 (see fig. 2). Late arrival times are observed on the volcano (up to 1.0 s.), suggesting a general delay on a broad crustal scale.

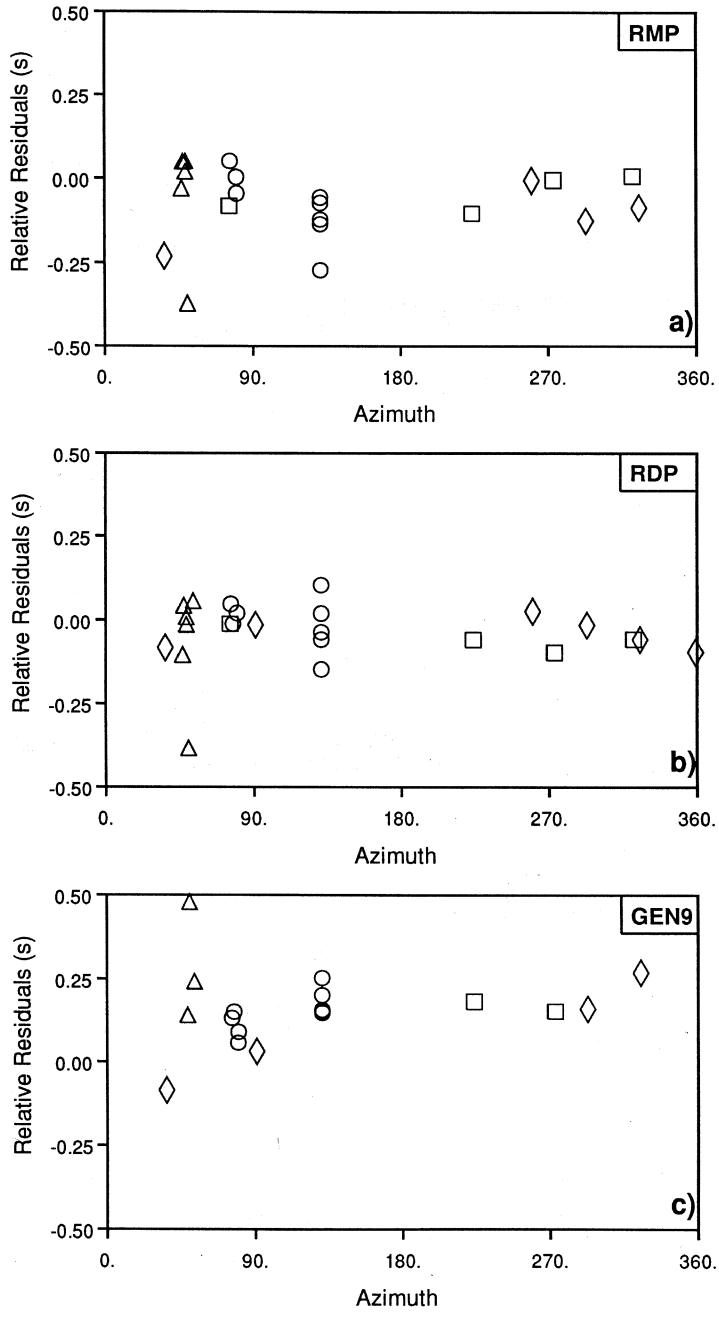

Fig. 8a-c. Azimuthal variation of the relative residuals (with respect to the network mean) obtained for (a) RMP, (b) RDP, and (c) GEN9 stations, located in the study area approximately on a N-S profile. Different symbols are used for epicentral distances between 25°-50° (circles), 50°-75° (squares), 75°-100° (diamond), and > 100° (triangles).

4. Three-dimensional inversion of relative residuals

To quantify the *P*-wave velocity perturbations beneath the volcano, we have inverted the relative residuals using a modified version of the ACH technique (Aki *et al.*, 1977; Ellsworth, 1977; Evans and Achauer, 1993).

According to this method, the investigated volume below the seismic array is parameterized with a series of homogeneous, constant velocity layers. Each layer is subdivided into a grid of rectangular blocks. The block sizes are primarily determined by the station spacing, and the wavelength of the teleseismic compressional waves (Ellsworth and Koyanagy, 1977). For our data set, these conditions suggest a block size of ~ 5-8 km.

The technique computes the travel times from the base of the laterally homogeneous starting model to the surface. Thus, for a single source-receiver pair, the travel time residual R_{ij}^{rel} can be related to the parameterized velocity model by means of

$$R_{ij}^{rel} = \sum_{k=1}^{NB} a_{ijk} \frac{\delta v_k}{v} \qquad (4.1)$$

where NB is the number of modelled blocks, a_{ijk} and $\delta v_k/v$ are the unperturbed travel times of ray ij and the unknown fractional velocity perturbations inside block k, respectively. Observations of relative residuals from a set of teleseismic events recorded across the seismic network, result in the linear system of equations

$$\boldsymbol{Am} = \boldsymbol{d} \qquad (4.2)$$

where $\boldsymbol{A}$ is the matrix containing the a_{ijk} terms, $\boldsymbol{m}$ and $\boldsymbol{d}$ are the unknown slowness changes and the residuals vector, respectively. Due to the existence of at least one zero eigenvalue for each layer of the initial model (Aki *et al.*, 1977; Ellsworth and Koyanagy, 1977), matrix $\boldsymbol{A}$ is singular and a direct least squares solution of (4.2) is not achievable. An estimate $\hat{\boldsymbol{m}}$ of the model parameters vector can be obtained using a damped least squares inversion scheme, according to the formula

$$\hat{\boldsymbol{m}} = (\boldsymbol{A}^T\boldsymbol{A} + \theta^2\boldsymbol{I})^{-1}\boldsymbol{A}^T\boldsymbol{d} \qquad (4.3)$$

where θ^2 is the damping parameter, and $\boldsymbol{I}$ is the identity matrix. An appropriate damping factor handles the singularity of matrix $\boldsymbol{A}$, balancing oversmoothing of real anomalies relative to noise in the data (Menke, 1989). A common method to choose θ^2, thus optimizing the inversion procedure, is to analise the trade-off between the data misfit and the model norm (see fig. 9a,b).

We parameterize the crustal structure of the Alban Hills volcano with two similar plane-parallel layer models, *direct* and *stripped* models, both extending to a depth of 23 km. The two models consist of four layers with velocity, thickness, number and horizontal size of the blocks, as specified in table I. The models differ in the application (or not) of a time correction to the blocks (station cones in the stripped model) of the first layer, to account for the shallowest geologic structure (Dawson *et al.*, 1990).

We choose the initial velocities considering geophysical and geological information on the crustal structure (Funiciello and Parotto, 1978; Chiarabba *et al.*, 1994) and the Herrin velocity model (Herrin, 1968) for the upper mantle. Block widths and layer thicknesses have been chosen by considering the mean station spacing (~ 5 km) and in order to obtain approximately constant travel times within the different layers (Evans and Achauer, 1993).

4.1. *Direct model*

In fig. 10a-d we show the velocity perturbations obtained by inverting the teleseismic data with the uncorrected four-layer crustal model (direct inversion). This model is the average of 9 inversions, performed shifting the grid one third of the block size in the x and y directions. This is done to avoid edge effects when an anomaly with a size similar to the block size is located close to a vertical boundary of the model (see Evans and Achauer, 1993). Initial data variance, remaining variance, and variance improvement achieved for this model with a damping factor of 20 s^2 (fig. 9) are 0.060 s^2, 0.031 s^2, and 49% respectively.

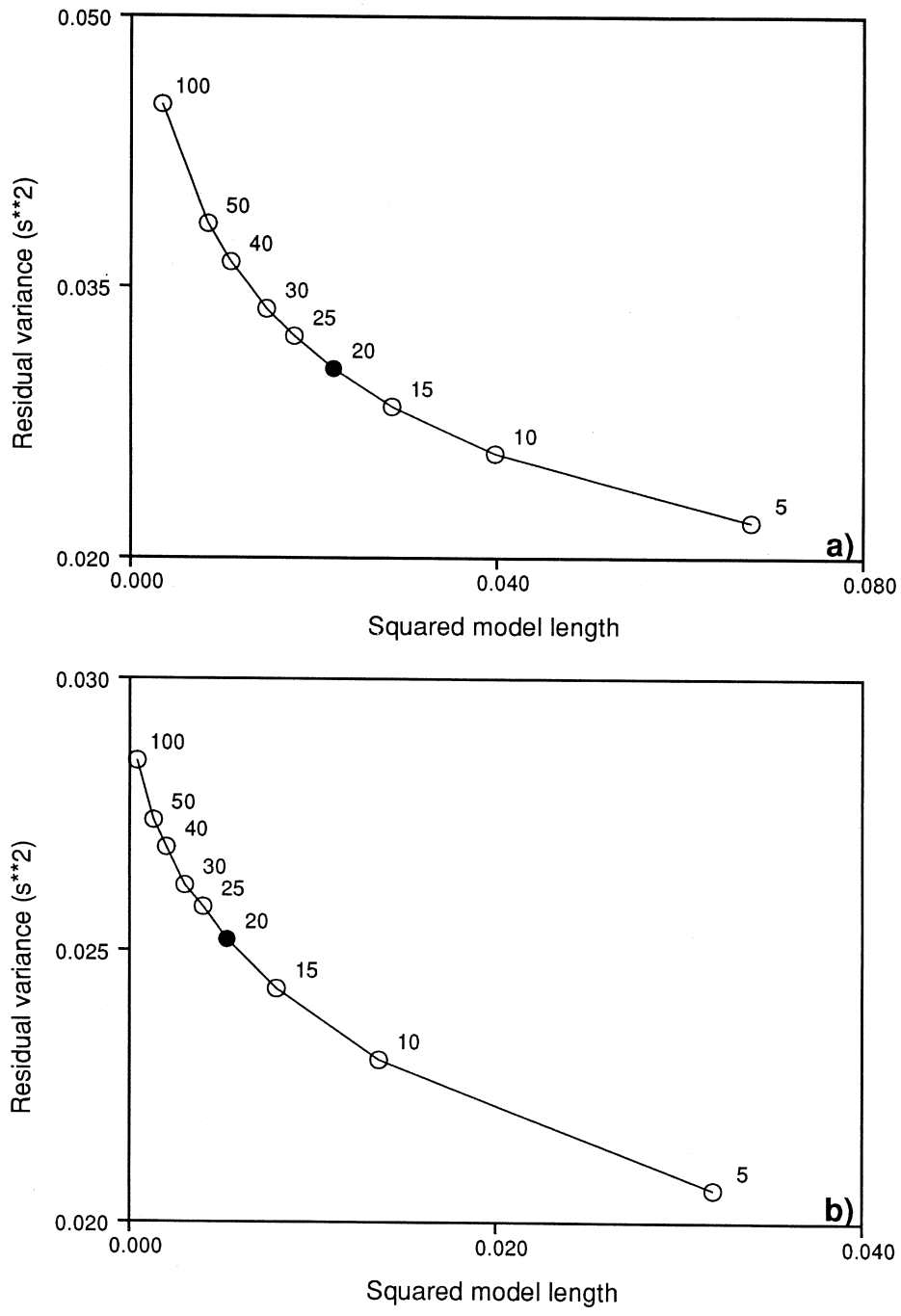

Fig. 9a,b. Trade-off between data variance and model length computed for the (a) direct and the (b) stripped model. Solid circles indicate the selected damping values.

Table I. Parameters of the initial model used in the direct and stripped inversions.

Layer	Initial velocity (km/s)	Thickness (km)	Block size (km × km)	Number of blocks (N-S) × (E-W)
1	5.00	5.0	5.0 × 5.0*	6 × 6
2	5.80	5.5	5.0 × 5.0	6 × 6
3	6.30	6.0	5.5 × 5.5	7 × 7
4	6.80	6.5	6.0 × 6.0	8 × 8

* Station cones in the *stripped* model.

In Layer 1 (0 to 5 km, fig. 10a) we observe a strong low velocity anomaly in the south-western side of the volcano, and a slight high velocity in the central area. This is consistent with the relative residual distribution. Velocity perturbations are on the order of ± 5% of the initial values. Associated standard errors are within ± 1.3% in the central part of the volcano. The low velocity region corresponds with the southermost craters of the latest activity of the volcano (0.20-0.030 Ma).

In Layer 2 (5 to 10.5 km, fig. 10b), the low velocity region beneath the phreato-magmatic craters is still evident, whereas the high velocity covers the region beneath the central cone.

In Layer 3 (10.5 to 16.5 km, fig. 10c) these two velocity features are spread over a larger area, toward the periphery of the model. In particular, the low-velocity anomaly present in Layer 2 beneath the phreato-magmatic craters is shifted toward south-east. The high velocity is still concentrated in the NE region, but the central region also appears to have higher velocity (fig. 10c).

In Layer 4 (16.5 to 23 km, fig. 10d) most of the velocity perturbations are located outside the volcano, reflecting poor ray sampling at these depths. These features, along with some intrinsic limitations linked to the tomographic inversion of teleseismic body wave data (as for instance less ability to image flat objects with respect to elongated bodies) (see Evans and Achauer, 1993), lead us to interpret the anomalies detected at this depth with caution. It appears that the main velocity anomalies in this model are confined in the upper three layers (~ 16 km). Major structural heterogeneities beneath the base of the model may determine the anomalies in the bottom layer of the model (Evans and Achauer, 1993).

4.2. *Stripped model*

Previous studies of the Alban Hills crustal structure have pointed out the existence of volcanic and sedimentary low-velocity materials overlaying the carbonate rocks at shallow depth, especially beneath the Ariccia crater and surrounding areas (Funiciello and Parotto, 1978; Chiarabba *et al.*, 1994). These materials produce a delay in the observed teleseismic residuals. The 3D inversion may smear this «shallow» delay into the deeper layers of the model, due to poor vertical resolution, intrinsic in any teleseismic inversion. In order to verify the effect of the low-velocity materials present close to the surface, we compare the 3D velocity images obtained by Chiarabba *et al.* (1994) inverting local earthquake data (fig. 11) with the first layer of the teleseismic model. A low velocity beneath Nemi and Ariccia craters and high velocity in the central part of the volcano are present in both models. However, we observe larger residuals on the teleseismic rays than in the local earthquake model. The observed residuals (see fig. 5) can not be explained only by structures close to the surface. This suggests that a considerable amount of the observed teleseismic residuals are generated by velocity heterogeneities deeper than ~ 5 km.

In order to remove the effect of the shallow materials present beneath the volcano, we

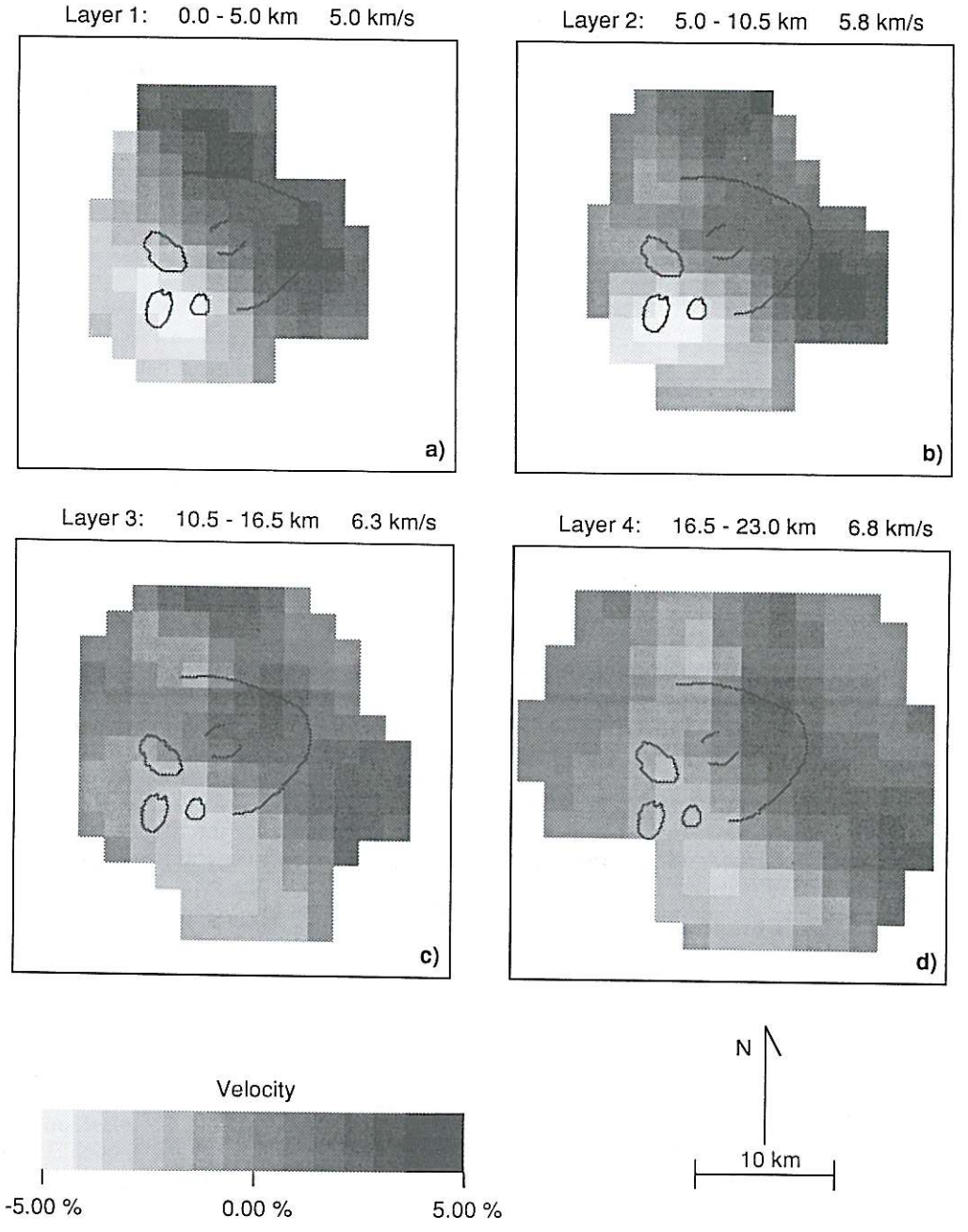

Fig. 10a-d. Velocity perturbations computed for the direct model. Note the two regions with high velocity beneath the east and the center of the volcano and a velocity decrease to the southwest. The results are derived from 9 inversions performed with the offset-and-average technique (see text and Evans and Achauer, 1993).

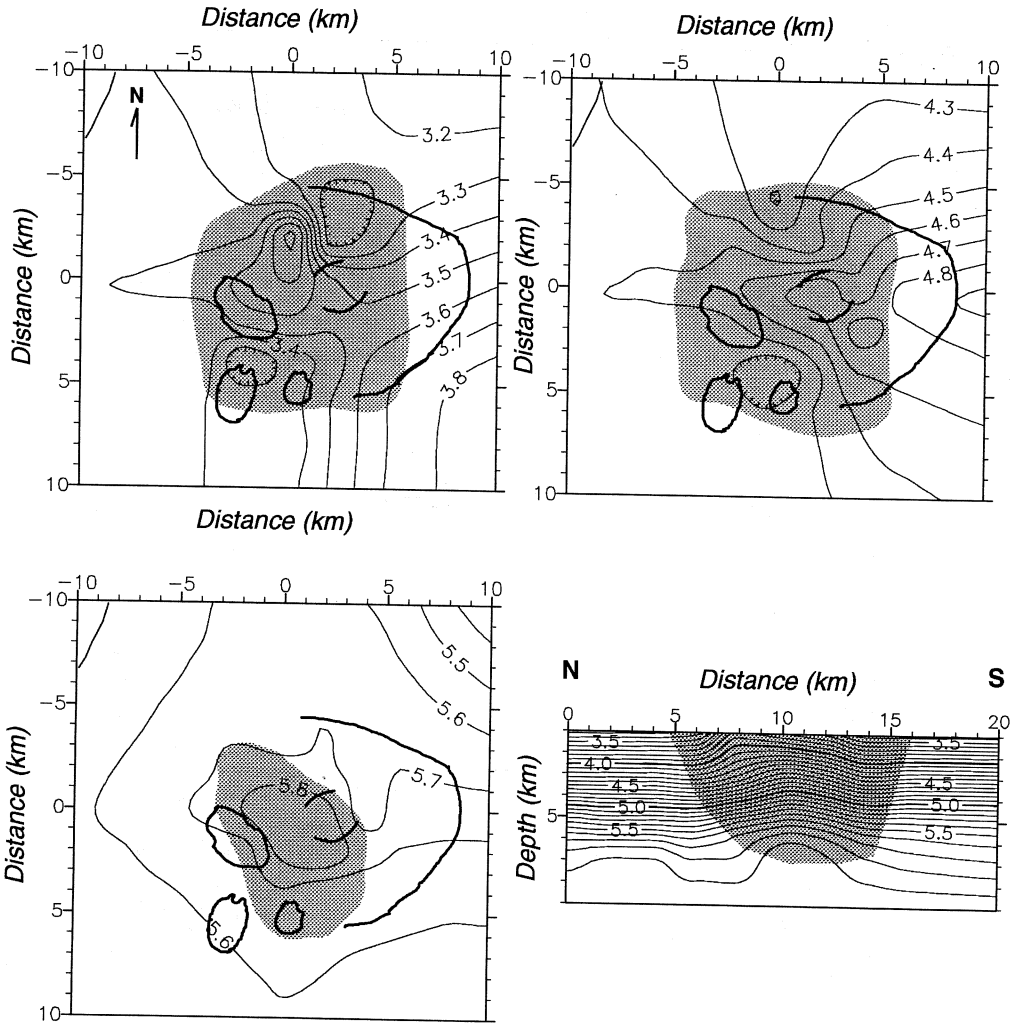

Fig. 11. Tomographic images obtained for the upper 6 km of the crust in the Alban Hills inverting the local earthquake data (from Chiarabba *et al.*, 1994). The shaded area depicts the well resolved region. Note the high-velocity anomaly at 6 km in the central region.

«strip» the velocity model computing station corrections with an iterative technique (Dawson *et al.*, 1990). The data were inverted with a one-layer velocity model (0 to 5 km depth), constituted by a cone for each station. The cone has the apex at the station, and the base at 5 km b.s.l., whereas its width (~ 6 km) is determined by the incidence angles of teleseismic rays (up to ~ 30°). The computed velocity perturbations are treated as station corrections and used as the input to several subsequent single-layer inversions. We invert the data until the first-layer corrections changed by less than 1%, a result that we reached after 5 inversions. Finally, we inverted the data with a three-dimensional model similar to the previous direct model (see table I), using the up-dated station corrections (ranging between + 15.9% in the

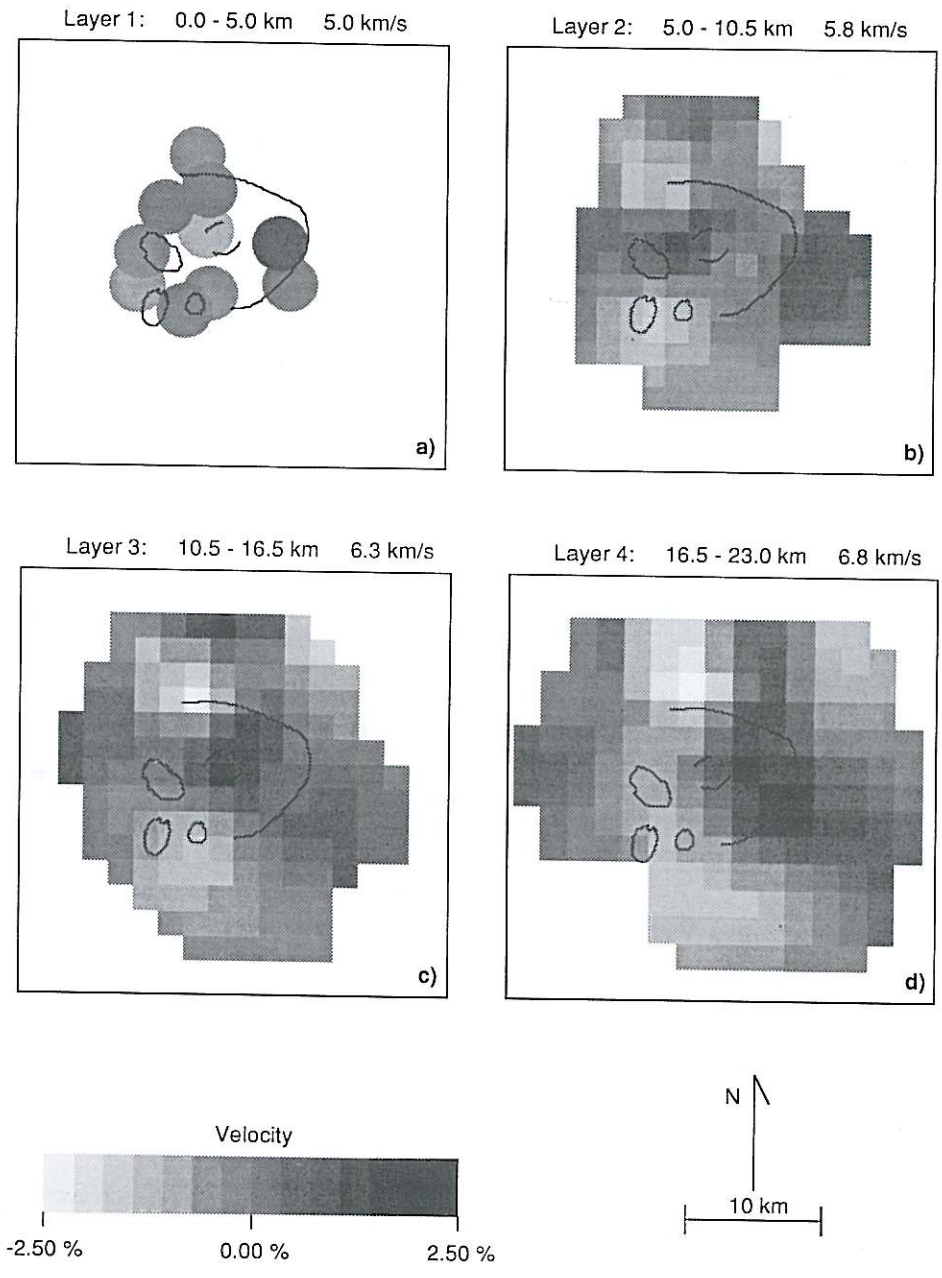

Fig. 12a-d. Velocity perturbations for the stripped model. Although the shallow anomalies are stripped by the procedure, we still observe the two anomalous regions imaged in the direct inversion. Note the strong similarity between the location of the high velocity anomaly in layer 2 (5-10.5 km) and the high velocity recovered by the local earthquake tomography (fig. 11). This anomaly seems to have deeper roots, as it is evident also in layer 3 (10.5-16.5 km).

NE region and − 15.7% for the SW stations). By doing so, we remove the contribution of the upper crustal structure (as station corrections) on the tomographic computation.

The results of the stripped inversion are shown in fig. 12a-d. Since the stripping tends to overestimate the contribution of shallow anomalies minimizing most of the residuals in the first layer (Dawson *et al.*, 1990), the imaged velocity perturbations appear smoother (± 2.5%) than the perturbation of the direct model. These first layer corrections reduce both the starting data variance (0.031 s^2) and the remaining variance (0.025 s^2), thus improving the fit of the computed model to the actual data.

In Layer 1, as expected, we do not observe lateral velocity contrast (fig. 12a), since we force the upper layer perturbations as station corrections. In Layer 2 two main anomalies appear. One is the low velocity beneath Ariccia and Nemi craters, the other is a high velocity beneath the central cone and the Albano Lake (fig. 12b). In Layer 3 the low velocity moves towards SE out of the well sampled area, although it still remains beneath the Nemi craters. The high-velocity zone beneath the central cone becomes more evident (fig. 12c). In Layer 4 (fig. 12d) the two primary anomalies are weaker, indicating that the heterogeneities are probably confined to the upper layers. However we must consider that the poor ray sampling can degrade the velocity image resolution below 16 km.

The stripped results suggest that significant anomalies exist at depth greater than 5 km, even if we constrain most of the relative residuals to occur in the shallow part of the model. In particular, as the vertical section of fig. 13a,b indicates, we can resolve the two different anomalies pointed out by the direct model, constraining their depth extension to about 16 km. The high velocity beneath the central cone is more evident when stripping the model, although its amplitude is not greater than + 2.0%. In fact we accommodate (as station corrections) part of the high-velocity anomaly present in the direct model outside the volcano in layer 1 (close to the south-eastern periphery) and smeared in layers 2 and 3 by the direct inversion. The stripping procedure seems to reduce the resolution artifacts.

Considering the poor ray sampling of the medium, and in order to assess the reliability of the tomographic images, we analyse the resolution and covariance matrices. In general, normalized diagonal elements of the resolution matrix $\boldsymbol{R}$ close to 1 indicate well resolved model parameters (Menke, 1989). In addition, a careful analysis of the off-diagonal elements of $\boldsymbol{R}$ helps to evaluate whether the velocity anomalies are smeared into adjacent blocks (Evans and Achauer, 1993). We find generally low values of the diagonal elements of $\boldsymbol{R}$ except for blocks in the central area (values close to 0.4). However, as shown in fig. 13b for an anomalous high velocity block in the third layer of the stripped model, the blocks appear to be well resolved at least in the horizontal direction as we do not observe substantial smearing into the adjacent blocks. Conversely, a slight vertical smearing occurs, as displayed by the resolution matrix (fig. 13b). Thus, the depth of the anomalies is poorly constrained by the tomographic inversion, but their horizontal position is well determined. The standard errors (the square root of the diagonal elements of the covariance matrix) associated with the velocity anomalies are on average of about ± 1%.

5. Discussion

Seismic tomographic experiments in volcanic regions have allowed different authors to infer the presence of structures such magma chambers, intrusive masses, and fluid enriched regions (*e.g.*, Iyer and Dawson, 1993 and references therein). The experimental observation that the increase of temperature decreases the velocity of compressional waves (Mavko, 1980; Sato *et al.*, 1989) represents the basis for the interpretation of velocity models beneath volcanoes. Thus, large low-velocity anomalies imaged beneath active or young volcanoes is attributed to the presence of hot magmatic bodies, generally interpreted as «magma chambers» (Iyer and Dawson, 1993). Conversely, high-velocity anomalies can represent congealed intrusive masses (Evans and Zucca, 1993).

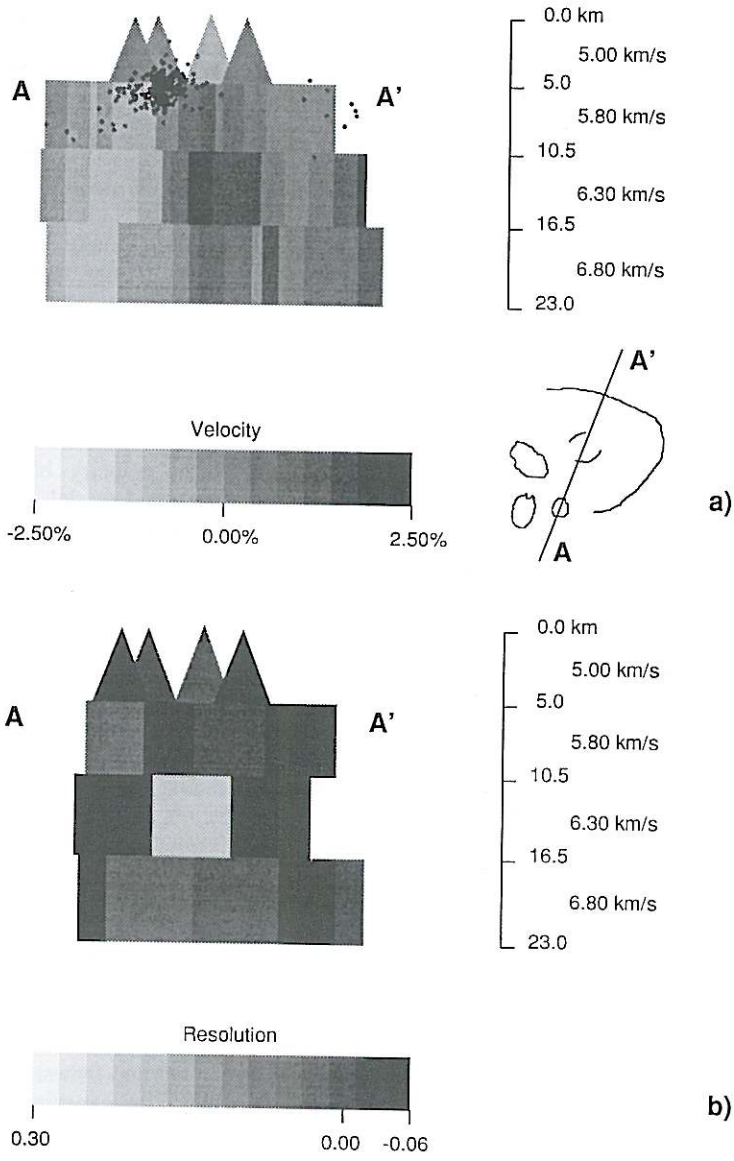

Fig. 13a,b. a) SSW-NNE cross-section computed for the stripped model. The low-velocity anomaly ranges between 5.0 and 16.5 km depth, whereas the high velocity zone is stronger between 10.5 and 16.5 km depth. Dots indicate hypocenters from a selected earthquake data set of the 1989-1990 seismic swarm (after Chiarabba *et al.*, 1994). b) Vertical section showing the column of the resolution matrix for a «fast» block in the third layer of the stripped model. The diagonal value in ***R*** for this block is 0.21, the velocity perturbation is + 1.45%, and the standard errors is ± 1.34%. The anomaly is slightly smeared in the vertical direction, as shown by the off-diagonal elements of the blocks above and beneath, as high as 0.1. Note that the block size is the real size used in the inversion (see table I), while in (a) (and in map views of figs. 10a-d and 12a-d) the blocks are smaller because of the offset-and-average procedure.

Numerous factors affect the seismic velocity and contribute to what we generally define as «velocity anomaly» (*e.g.*, Kern, 1982; Nur, 1987). Thus the interpretation of tomograms needs a joint analysis of all available geological and geophysical information in order to constrain the proposed model. Unfortunately, we can only rely on few deep structural data available for the Alban Hills. In particular, an uplifted limestone unit (Funiciello and Parotto, 1978) was hypothesized in the upper 6 km of the crust beneath the north-western side of the volcano on the basis of gravity data and on the analysis of ejecta included in the volcanic rocks. The limestones are probably metamorphosed at 6 km depth, and a plexus of dikes, related to the top of a crystallized intrusion, is hypothesized by Chiarabba *et al.* (1994), based on tomographic and seismological studies.

With regard to our teleseismic tomographic results, since the vertical resolution of the tomographic images is poor, we cannot achieve detailed information about the geometry and dimensions of the imaged heterogeneous zones. The low velocity region detected beneath the western side of the volcano (figs. 5a,b, 6, 10a-d, 12a-d, and 13a) corresponds with the most recent craters (0.030-0.20 Ma), and is close to the area where the seismicity is located (fig. 13a). The amplitude of this anomaly is relatively weak, – 6.7% in the direct and – 2.4% in the stripped model. In this area the brittle/ductile transition is hypothesized at ~ 6 km (Amato *et al.*, 1994), suggesting that the crust at this depth is at temperature higher than 400-500°. Thus we prefer to interpret the low velocity anomaly detected by the teleseismic inversion at depth of ~ 5-16 km either as a small magma chamber (that we are not able to resolve in detail with the present data geometry), or to a diffuse higher temperature region generated by a deeper thermal source. A decrease in compressional wave velocities can be determined by a few percent of melt in the rocks (Mavko, 1980; Sato *et al.*, 1989; Iyer and Dawson, 1993).

The high velocities beneath the central part of the Alban Hills can be related to the cold lithospheric roots of the volcano (figs. 12a-d and 13a), remnants of the former magmatic activity (0.7-0.3 Ma). Since the roots appear to be confined to layers 2 and 3 (5.0-16.5 km depth), we may argue that they are not connected with an upper mantle source. For the stripped model the amplitude of this positive anomaly is as high as + 2.0% in the region of greater resolution.

6. Conclusions

The analysis of teleseismic travel time residuals provides new information on the crustal heterogeneities beneath the Alban Hills volcano. In particular, we observe large *P*-wave residual variations (up to 0.6 s) between stations located on the southwestern side of the volcano (delayed arrivals) with respect to the stations on the central and northern part (early arrivals). Delayed arrivals correspond to a low-velocity zone beneath the most recent phreatomagmatic craters, whereas early arrivals are relative to high velocities beneath the central cone. A general delay is also observed for all the stations on the volcano with respect to the close Apenninic margin (CP9 station), suggesting that a low-velocity anomaly may characterize the Alban Hills on a broader scale (whole crust and/or upper mantle).

Three-dimensional images, although not well constrained by the poor ray sampling, delineates the anomalous low-velocity region beneath the Albano and Nemi craters to the southwest of the central volcano. We propose that the decrease of *P*-wave velocity in this region is due to the presence of a remnant magmatic body in the crust (approximatively between 5 km and 16 km depth). Local earthquake tomography indicates that a high-velocity body is present beneath the north-western part of the Alban Hills from the surface up to 6 km depth. This positive anomaly, which extends toward the center of the volcano at 6 km depth, corresponds to the high-velocity anomaly defined by the teleseismic rays beneath the central cone. We interpret the high-velocity volume as due to the old (0.7-0.3 Ma) intrusive roots of the central activity of the Alban Hills volcanic system.

Acknowledgements

The authors gratefully acknowledge P.B. Dawson, M. Cocco, and an anonymous reviewer for useful criticism. We are indebted to J. Coakley and M. Scardella for help in field work.

REFERENCES

Aki, K., A. Christoffersson and E.S. Husebye (1977): Determination of the three-dimensional seismic structure of the lithosphere, *J. Geophys. Res.*, **82**, 277-296.

Amato, A. and G. Valensise (1986): Il basamento sedimentario dell'area albana: risultati di uno studio degli «Ejecta» dei crateri idromagmatici di Albano e Nemi, *Mem. Soc. Geol. It.*, **35**, 761-767 (in Italian).

Amato, A., B. Alessandrini and G.B. Cimini (1993): Teleseismic wave tomography of Italy, in *Seismic Tomography: Theory and Practice*, edited by H.M. Iyer and K. Hirahara (Chapman and Hall, London), 361-397.

Amato, A., C. Chiarabba, M. Cocco, M. Di Bona and G. Selvaggi (1994): The 1989-1990 seismic swarm in the Alban Hills volcanic area, Central Italy, *Journal of Volcanology and Geothermal Res.* (in press).

Bertagnini, A., D. De Rita, R. Funiciello, A. Sbrana and R. Trigila (1985): The Latium volcanism, Excursion Guidebook IAVCEI, 32-39.

Chiarabba, C., L. Malagnini and A. Amato (1994): Three-dimensional velocity structure and earthquake relocation in the Alban Hills volcano, Central Italy, *Bull. Seismol. Soc. Am.* (in press).

Cimini, G.B. and A. Amato (1993): *P*-wave teleseismic tomography: contribution to the delineation of the upper mantle structure of Italy, in *Recent Evolution and Seismicity of the Mediterranean Region*, edited by E. Boschi, E. Mantovani and A. Morelli (Kluwer Academic Publishers, Dordrecht), 313-331.

Dawson, P.B., J.R. Evans and H.M. Iyer (1990): Velocity structure of the crust and upper mantle beneath Long Valley Caldera, California, *J. Geophys. Res.*, **95**, 11201-11050.

De Rita, D., R. Funiciello and M. Parotto (1988): Geological Map of the Colli Albani Volcanic complex («Vulcano Laziale»), CNR-GNV, Joint Venture ENEL-AGIP.

Ellsworth, W.L. (1977): Three-dimensional structure of the crust and mantle beneath the island of Hawaii, Ph.D. thesis (Mass. Inst. of Technol., Cambridge), pp. 237.

Ellsworth, W.L. and R.Y. Koyanagy (1977): Three-dimensional crust and mantle structure of Kilauea volcano, Hawaii. *J. Geophys. Res.*, **82**, 5379-5394.

Evans, J.R. and U. Achauer (1993): Teleseismic velocity tomography using the ACH method: theory and application to continental-scale studies, in *Seismic Tomography: Theory and Practice*, edited by H.M. Iyer and K. Hirahara (Chapman and Hall, London), 319-360.

Evans, J.R. and J.J. Zucca (1988): Active high resolution seismic tomography of compressional wave velocity and attenuation structure at Medicine Lake volcano, Northern California, *J. Geophys. Res.*, **93**, 15016-15036.

Fornaseri, M. (1985): Geochronology of volcanic rocks from Latium (Italy), *Rend. Soc. It. Min. Petrol.*, **4**, 73-106.

Funiciello, R. and M. Parotto (1978): Il substrato sedimentario nell'area dei Colli Albani: considerazioni geodinamiche e paleogeografiche sul margine tirrenico dell'Appennino Centrale, *Geol. Rom.*, **17**, 233-287 (in Italian).

Harris, R.A., H.M. Iyer and P.B. Dawson (1991): Imaging the Juan de Fuca plate beneath Southern Oregon using teleseismic *P* wave residuals, *J. Geophys. Res.*, **96**, 19879-19889.

Herrin, E. (1968): Introduction to «1968 seismological tables for *P* phases», *Bull. Seismol. Soc. Am.*, **58**, 1193-1242.

Iyer, H.M. and P.B. Dawson (1993): Imaging volcanoes using teleseismic tomography, in *Seismic Tomography: Theory and Practice*, edited by H.M. Iyer and K. Hirahara (Chapman and Hall, London), 466-492.

Kern, H. (1982): *P*- and *S*-wave velocities in crustal and mantle rocks under the simultaneous action of high confining pressure and high temperature and the effect of the rock microstructure, in *High-Pressure Researches in Geoscience*, edited by W. Schreyer (E. Schweizerbart'sche Verlagsbuch-handlung, Stuttgart), 13-45.

Mavko, G.M. (1980): Velocity and attenuation in partially molten rocks, *J. Geophys. Res*, **85**, 5173-5189.

Menke, W. (1989): Geophysical data analysis: discrete inverse theory, *International Geophysics Series*, (Academic Press, Inc.) **45**, pp. 285.

Molin, D. (1981): Sulla sismicità storica dei Colli Albani, *Comitato Nazionale Energia Nucleare*, CNEN-RT/AMB(81)11 (in Italian).

Nur, A. (1987): Seismic rock properties for reservoir descriptions and monitoring, in *Seismic Tomography with Applications in Global and Exploration Geophysics*, edited by G. Nolet, (Reidel, Hingham, MA), 203-237.

Sato, H., I.S. Sacks and T. Murase (1989): The use of laboratory velocity data for estimating temperature and partial melt fraction in the low-velocity zone: comparison with heat flow and electrical conductivity studies, *J. Geophys. Res*, **94** (5), 689-704.

Steeples, D.W. and H.M. Iyer (1976): Low-velocity zone under Long Valley as determinated from teleseismic events, *J. Geophys. Res*, **81**, 335-341.

Toro, B. (1977): Gravimetry and deep structure of the Sabatinian and Alban volcanic areas (Latium), *Geol. Rom.*, **15**, 301-310.

(received April 7, 1994;
accepted July 29, 1994)